Microstructure and mechanical properties of electroplated Ni-Sn TLP bonded joints with different bonding and aging times

Guangxu Yan[a], Vincent Gill[c], Chee Lip Gan[a,b]*, Zhong Chen[a,b]*

[a] Rolls-Royce@NTU Corporate Lab, Nanyang Technological University, 50 Nanyang Avenue, Singapore 639798, Singapore

[b] School of Materials Science and Engineering, Nanyang Technological University, 50 Nanyang Avenue, Singapore 639798, Singapore

[c] Rolls-Royce Singapore Pte Ltd, 1 Seletar Aerospace Crescent, Singapore 797565, Singapore

*Corresponding authors

E-mail addresses: clgan@ntu.edu.sg (Chee Lip Gan); aszchen@ntu.edu.sg (Zhong Chen)

Abstract

Much attention has been drawn to the Ni-Sn transient liquid phase (TLP) bonded joints for high-temperature electronic packaging applications since their inception. A comparative study of Ni-Sn TLP bonded joints with different interlayers was conducted. The evolution of microstructure and mechanical properties of joints with different bonding times was also investigated. In addition, the high-temperature (300 °C) thermal reliability of the Ni-Sn TLP bonded joints was explored with aging times from 0 h to 100 h. The results show that electroplated Ni-Sn TLP bonded joints exhibited a slightly higher average shear strength than those prepared using Sn foil and $Sn_{96.5}Ag_{3.5}$ paste. Also, the average shear strength of the electroplated Ni-Sn TLP bonded joints was greatly improved when the bonding time increased from 0.5 h to 5 h, while there was a continuous decrease in the average shear strength as the aging time was increased from 4 h to 100 h. During aging, the Ni/Ni_3Sn_2 interface was the preferential site for the nucleation of newly formed Ni_3Sn_2 intermetallic compounds (IMCs). Furthermore, the cross-sectional microstructure of the shear fractured joints after aging from 4 h to 100 h indicates that the shear fractures propagated through both the Ni_3Sn_4 IMCs and the Ni_3Sn_2/Ni_3Sn_4 interface.

Keywords: Ni-Sn TLP bonding, Microstructure, Mechanical properties, Thermal reliability, High-temperature electronic packaging

1 Introduction

To cope with the challenges in replacing high-Pb solders and creating solid bonds for harsh environmental electronic applications, transient liquid phase (TLP) bonding has been widely explored, especially for high-temperature electronic packaging [1, 2]. TLP bonds can be processed at relatively low temperatures while being used at higher temperatures through the formation of intermetallic compounds (IMCs). Many material systems (such as Cu-Sn, Ag-Sn, Ni-Sn, Ag-Cu-Sn, Cu-Ni-Sn, and Sn-Bi with Cu, Ni or Ag) have been investigated for TLP bonding in electronic packaging [2-4]. Among these, the Cu-Sn [5-7], Ag-Sn [8, 9], Ni-Sn [10] and Cu-Ni-Sn [11, 12] are the most promising metallic systems for high-temperature electronic packaging applications [13]. Joints with excellent mechanical strengths can be obtained in the

Cu-Sn and Ag-Sn TLP material systems due to the formation of Cu_3Sn and Ag_3Sn IMCs, respectively. However, the formation of Kirkendall voids during Cu-Sn TLP bonding can hardly be avoided due to the phase transformation from Cu_3Sn to Cu_5Sn_6, which in turn deteriorates the thermal reliability of the joint [14]. Besides, joints with Ag_3Sn IMCs cannot withstand high temperatures beyond 480 °C [15]. In contrast, Ni-Sn TLP bonded joints with Ni_3Sn_4 IMCs have satisfactory mechanical strengths and can withstand high temperatures up to 794.5 °C. However, it is quite challenging to obtain Ni-Sn TLP bonded joints with expected microstructure and satisfactory thermal reliability, since the performance highly depends on the substrate, deposition process, interlayer morphology and bonding profile. Therefore, further investigation of Ni-Sn TLP bonding for high-temperature electronic packaging is required [16].

Many studies have been conducted for Ni-Sn TLP bonded joints. Shen et al. [17] investigated the growth mechanism of Ni_3Sn_4 IMCs in Ni-Sn TLP bonds. They used button-shaped Sn-enriched solder alloys as the interlayer and found that the growth of Ni_3Sn_4 was affected by grain boundary diffusion, volume diffusion, grain boundary grooving, coarsening and dissolution into the molten solder. Li et al. [16] investigated the effects of ultrasound-induced TLP bonding on the microstructure and mechanical strength evolution of Ni-Sn foil TLP bonded joints and claimed that the ultrasound-induced TLP process accelerated the formation of Ni_3Sn_4 during bonding. The ultrasonic processing also refined the grains of Ni_3Sn_4 IMCs, which resulted in an increase in the average shear strength of joints compared to that of the joints bonded in the traditional reflow oven. Jeong et al. [18] evaluated the long-term reliability of 30Ni-70Sn TLP bonded joints using solder paste containing Ni and Sn powders and proved their superior mechanical properties after long-term aging (1000 h) at a relatively high temperature (up to 200 ℃). Based on these research works, it is known that Sn-enriched solder alloys, Sn foil, and Sn-enriched paste have been widely used as the interlayers for Ni-Sn TLP bonding for high-temperature electronic packaging. However, high-quality thin Sn foils and Sn-enriched solder alloys are costly, and the thickness of these interlayers is hard to control. Besides, it is challenging to adjust the amount of Sn-enriched paste applied for the TLP bonding. Too much Sn should be avoided as it can result in excess Sn after bonding or a prolonged bonding time. A large amount of remnant Sn deteriorates the mechanical strength of the Ni-Sn joint. Sputtered Sn also has been used as the interlayer for Ni-Sn TLP bonding though its deposition rate is limited [19]. However, it is inappropriate where a relatively thick Sn layer is required [20]. To cope with these issues, the cost-effective and efficient electroplating was introduced to deposit the Ni-Sn layers.

To date, limited research has been conducted on electroplated Ni-Sn TLP bonded joints. Chuang et al. [21] studied electroplated Ni-Sn TLP bonded joints with different thicknesses of Sn at different aging times and concluded that the voids formed in the joint were due to the volume shrinkage caused by phase transformation. They also studied the effect of the addition of a small amount of Ag and found that the formation of voids can be effectively inhibited with the addition of 2.4 wt.% of Ag. In addition, Lis et al. [22] investigated the formation and growth of Ni_3Sn_4 IMCs in electroplated Ni-Sn TLP bonded joints and demonstrated that a diffusion barrier formed as a needle-like IMC layer densified around the Ni/Ni_3Sn_4 interface after bonding for 180 s. The aforementioned research provides important findings on the

mechanisms of the formation of voids and the growth of Ni_3Sn_4 IMCs in electroplated Ni-Sn TLP bonded joints. Until now, limited research has explored the evolution of microstructure and mechanical strength of electroplated Ni-Sn TLP bonded joints with various bonding and aging times at a high temperature of 300 °C, the failure mechanisms during shear tests and how they correlate with the mechanical properties of the joints.

In the present study, electroplated Ni-Sn TLP bonding joints were studied for potential high-temperature electronic packaging applications. A comparative study of microstructure, average shear strengths and fracture morphologies of Ni-Sn joints made using different interlayers (Sn foil, $Sn_{96.5}Ag_{3.5}$ paste and the electroplated Sn) was conducted. The microstructure and mechanical strength evolution of electroplated Ni-Sn joints prepared under different bonding times were also characterized and analysed. In addition, the thermal reliability of the electroplated Ni-Sn TLP bonded joints after aging at 300 °C for different times was investigated. Furthermore, fracture morphologies of the electroplated Ni-Sn TLP bonded joints were characterized and correlated with the microstructure and shear strengths to analyze the fracture mechanisms of the joints.

2 Experimental setup and materials

Commercial alumina plates (50 × 50 × 0.6 mm^3, 96% purity, from ACME Research Support Pte Ltd.) were selected as the bonding substrates. The surface roughness of the alumina is around 0.8 μm Ra, and a typical 3D surface roughness profile (taken from LEXT OLS4100 3D measuring laser microscope) is shown in Fig. 1. The alumina plates were thoroughly cleaned with DI water and acetone in an ultrasonic cleaner. Firstly, a thin layer (around 300 nm) of Ti was deposited on the alumina substrate by physical vapor deposition (PVD) (on a Kurt J Lesker PVD 75 sputter deposition system). This Ti layer acted as a barrier, adhesion and conductive layer. After that, the deposited alumina plates were diced into 10 × 20 mm^2 samples for electroplating. Electroplating of Ni and Sn was carried out in a Watts bath and an acidic sulfate bath, respectively. The corresponding chemical compositions for the electroplating are shown in Table 1. The electroplating current densities were set at 5-6 Adm^{-2} and 2.5-3 Adm^{-2} for the deposition of Ni and Sn, respectively. A typical single side of the alumina plate with the electroplated Ni and Sn layers is shown in Fig. 2(a). Other interlayer solders such as Sn foil and $Sn_{96.5}Ag_{3.5}$ paste were used for the comparative study as well. The electroplated samples were diced into 5 × 5 mm^2 (top side) and 10 × 10 mm^2 (bottom side) plates for the TLP bonding. After assembling the joints, the samples were locked in a stainless steel mould with a preload of around 40 MPa to maintain the thickness of the joints in a defined range and to minimise void formation during bonding. Fig. 2(b) shows a schematic of the bonding structure for the electroplated Ni-Sn TLP joint used to bond alumina onto alumina. The assembled samples were heated to 300 °C with a ramping up rate of 10 °C/min. The samples were soaked at 300 °C for 2 h for the comparative study of Ni-Sn TLP bonding joints using different interlayers. Additional samples were soaked at 300 °C for 0.5 h, 1 h, 2 h, and 5 h to investigate the effect of bonding time on the microstructure and mechanical strength evolution of the electroplated Ni-Sn TLP bonded joints. All these samples were bonded in a horizontal split tube furnace (Carbolite HST 12/300) with an argon protective atmosphere and cooled to room temperature by furnace cooling. Some of the as-bonded samples (bonded at 300 °C for 1 h) were aged at 300 °C for 4 h, 10 h, 25 h, 50 h and 100 h in an atmospheric oven (Memmert oven 100-800) for the thermal reliability tests. The bonded and aged Ni-Sn joints were ground using SiC

sandpaper with grits from ×320 to ×1000 followed by polishing with DiaPro Dac/Dur suspensions and a standard fumed silica suspension. The scanning electron microscope (SEM) image of the single side alumina substrate with the deposited Ni and Sn layers was taken on a FESEM 7600F, while the backscatter electron (BSE) images, energy-dispersive spectroscopy (EDS) and electron backscatter diffraction (EBSD) characterizations were conducted on a FESEM 7800F. The shear tests were conducted using a Dage 4000 Bondtester according to the MIL-STD-883 method 2019 test standard. For each condition, 5 to 8 samples were tested to obtain the average shear strength.

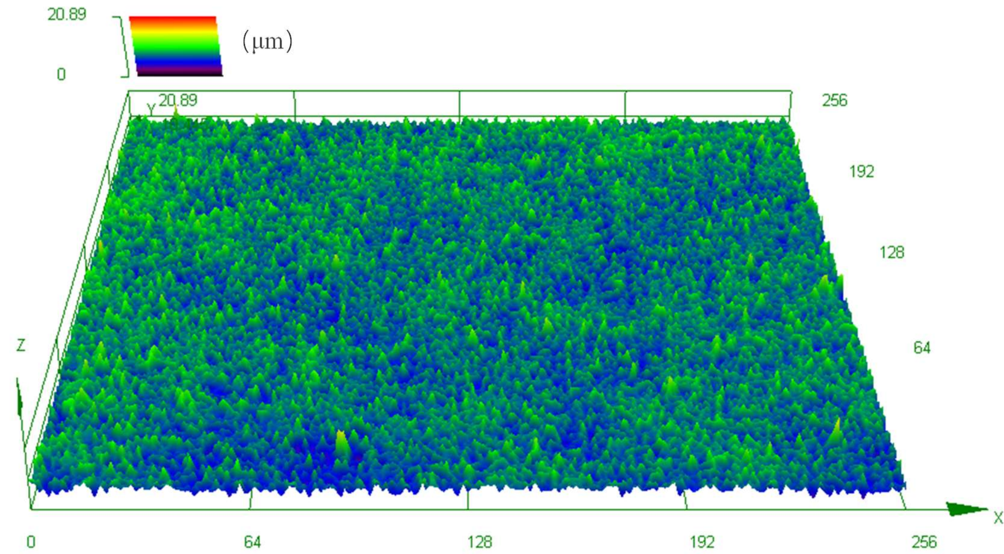

Fig. 1. 3D surface roughness profile of the alumina plate.

Table 1. The bath compositions used for electroplating Ni and Sn.

Watts bath (for Ni)	$NiCl_2 \cdot 6H_2O$ (60 g/L)	$NiSO_4 \cdot 6H_2O$ (300 g/L)	H_3BO_3 (40 g/L)
Acidic sulfate bath (for Sn)	$SnSO_4$ (30 g/L)	H_2SO_4 (200 g/L)	Triton X-100 (0.1 g/L)

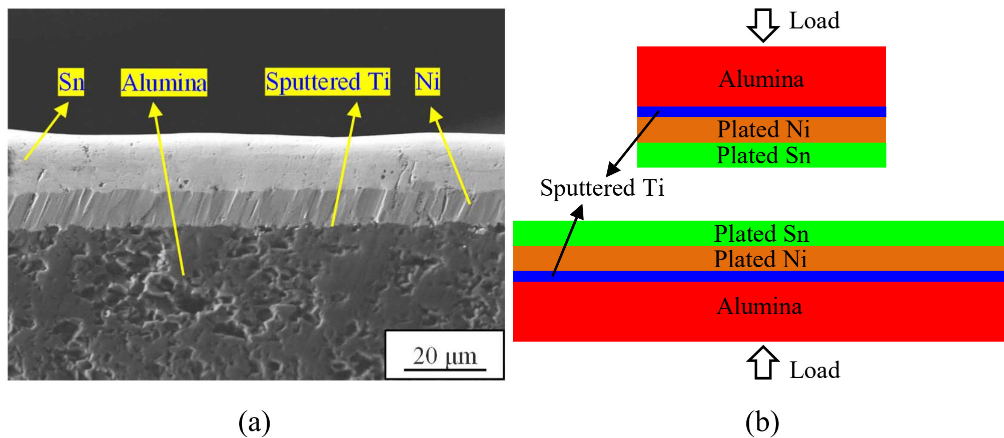

(a) (b)

Fig. 2. (a) Cross-sectional SEM image of the alumina plate with the sputtered Ti, electroplated Ni and Sn layers, and (b) schematic of the bonding structure for the electroplated Ni-Sn TLP bonded joint used to bond alumina onto alumina.

3 Results and discussion

3.1 Comparison of Ni-Sn TLP bonded joints with different interlayers

Based on the aforementioned studies, a variety of different Sn-enriched interlayers have been used for Ni-Sn TLP bonding. Besides electroplated Sn, these include Sn foil and Sn-enriched paste [16, 18]. The schematics of bonding structures for the Ni-Sn TLP bonded joints that used Sn foil and $Sn_{96.5}Ag_{3.5}$ paste are shown in Fig. 3(a) and (b), respectively. BSE images of the localized areas of Sn foil and $Sn_{96.5}Ag_{3.5}$ paste are shown in Fig. 3(c) and (d). It can be observed that there are initial voids in the Sn foil and the thickness of the Sn foil is around 25-30 µm. The paste is a mixture of flux and $Sn_{96.5}Ag_{3.5}$ particles with diameters in the range of 10-30 µm.

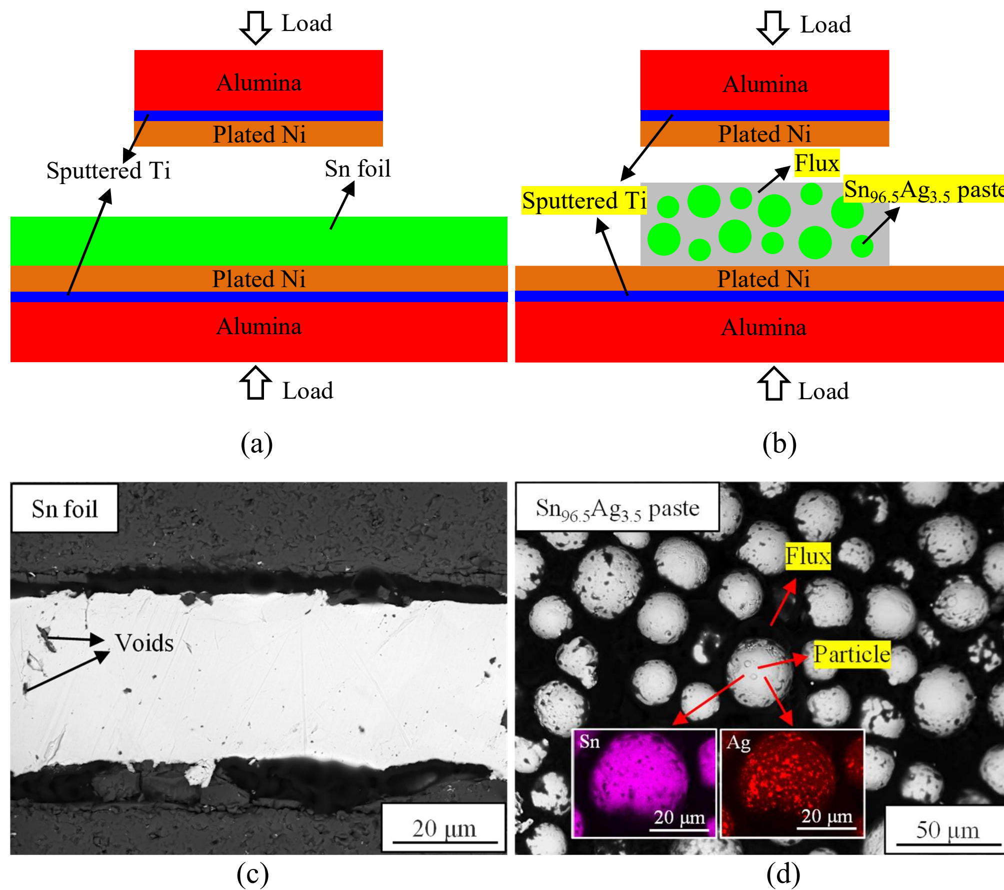

Fig. 3. Schematics of bonding structures for the Ni-Sn TLP bonded joints made using (a) Sn foil, (b) $Sn_{96.5}Ag_{3.5}$ paste as interlayers, and BSE images of (c) Sn foil and (d) $Sn_{96.5}Ag_{3.5}$ paste.

As cohesive failures only occurred in areas of the joints containing IMCs, this work focuses on regions with IMCs (with/without remnant Sn) rather than areas of Ni and alumina. EBSD characterization of IMCs and remnant Sn are highlighted while the remaining regions of the joint are displayed as band contrast images. Fig. 4 shows the combined band contrast and phase mappings of the cross-sectional microstructure of Ni-Sn TLP bonded joints that used different

interlayers. It can be observed that there was remnant Sn (purple) in all the bonded joints (after bonding at 300 °C for 2 h) and the remnant Sn accumulated around the grain boundaries of the Ni_3Sn_4 IMCs (yellow). In addition, obvious voids were found in the joints made using Sn foil (Fig. 4(a)) and $Sn_{96.5}Ag_{3.5}$ paste (Fig. 4(b)), while fewer voids were observed in the joints made using electroplated Sn (Fig. 4(c)). Voids within and around the Ni_3Sn_4 IMC grains of the Sn foil joint, can be attributed to the preexisting voids in the Sn foil (as shown in Fig. 3(c)) and the volume shrinkage caused by the phase transformation during bonding. While voids in the $Sn_{96.5}Ag_{3.5}$ paste joint can be attributed to the combined effects of flux evaporation and volume shrinkage during bonding. It is challenging to control the amount of the $Sn_{96.5}Ag_{3.5}$ paste applied during assembling. A relatively large amount of $Sn_{96.5}Ag_{3.5}$ paste can lead to excess Sn. On the other hand, the thickness of the electroplated Sn layer can be precisely controlled. Little to no remnant Sn was achieved in electroplated Ni-Sn TLP bonded joints through the adjustment of electroplating parameters. The inverse pole figure (IPF-Y, the normal reaction direction of the Ni-Sn joint) mappings in Fig. 4 show that there is no preferred orientation of the Ni_3Sn_4 IMC grains formed in all joints. In addition, kernel average misorientation (KAM) mappings of the joints show that the local average misorientations adjacent to the voids and remnant Sn regions were higher than in other areas. Higher local average misorientation angles indicate relatively larger strain deformation, which corresponds to higher stress concentrations [23, 24]. The higher stress around the remnant Sn regions might result from the phase mismatch and there was enough energy accumulated in these sites for dislocation motion and rearrangement to nucleate the newly formed fine Ni_3Sn_4 IMC grains [23].

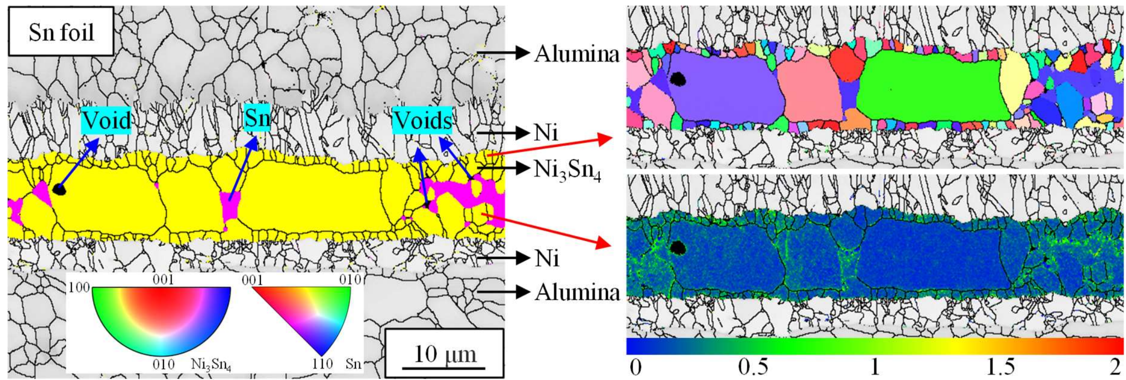

(a)

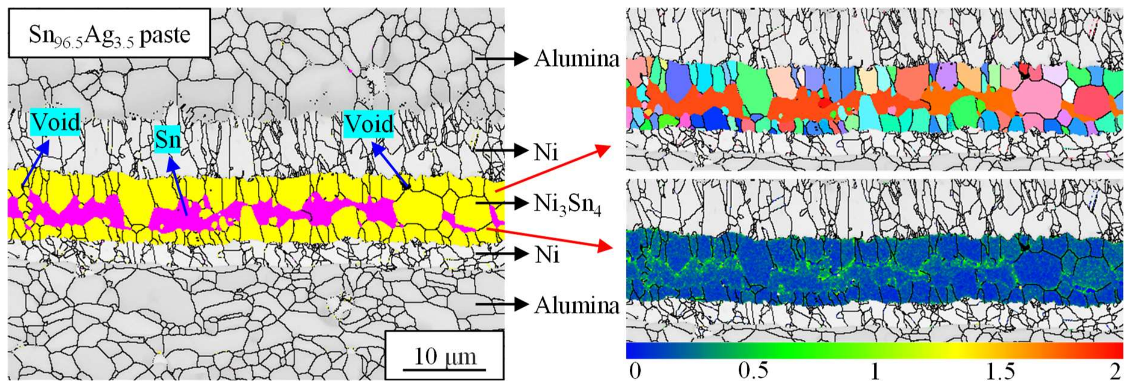

(b)

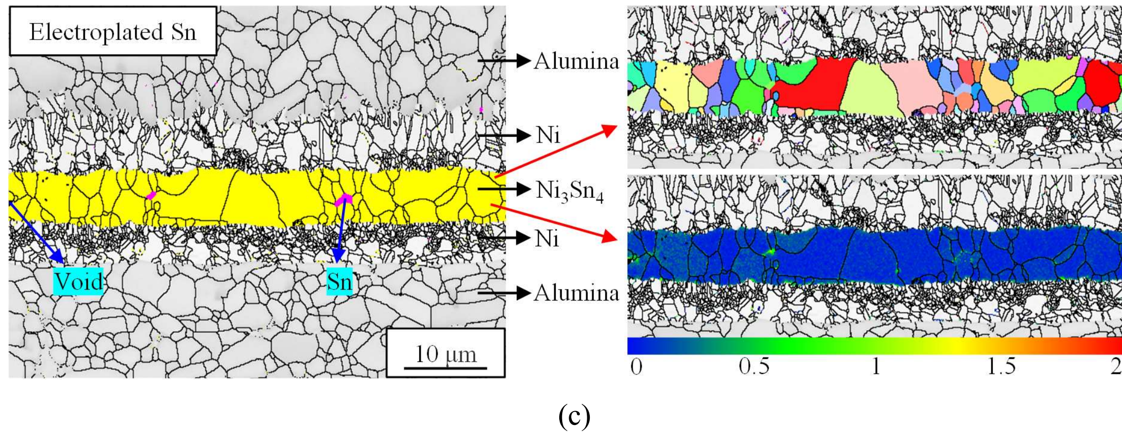

(c)

Fig. 4 Combined band contrast, phase, IPF(Y) and KAM mappings of the cross-sectional microstructure of Ni-Sn TLP bonding joints made using different interlayers, (a) Sn foil, (b) $Sn_{96.5}Ag_{3.5}$ paste, and (c) electroplated Sn (bonded at 300 °C for 2 h).

Fig. 5 shows that the average shear strengths of the Ni-Sn TLP bonded joints made using Sn foil, $Sn_{96.5}Ag_{3.5}$ paste and electroplated Sn are 17.74 ± 3.19 MPa, 18.90 ± 5.03 MPa and 21.65 ± 3.37 MPa, respectively. The average shear strength of the joints prepared using Sn foil is slightly lower than others, which was likely the result of preexisting voids in the commercial Sn foil (as shown in Fig. 3(c)) that resulted in relatively more voids in the bonded joints which in turn, acted as crack initiation sites during shear tests. In addition, the relatively larger variation in the shear strength profile of the joints made using $Sn_{96.5}Ag_{3.5}$ paste was due to the difficulty in controlling the amount of paste applied for TLP bonding. Too much paste led to a relatively larger amount of remnant Sn in the joint, which resulted in lower shear strength. On the contrary, the joints that employed the electroplated Sn as the interlayer show a relatively higher average shear strength as the thickness of the electroplated Sn layer can be controlled more precisely and only a little or even no Sn remained in the joint after TLP bonding.

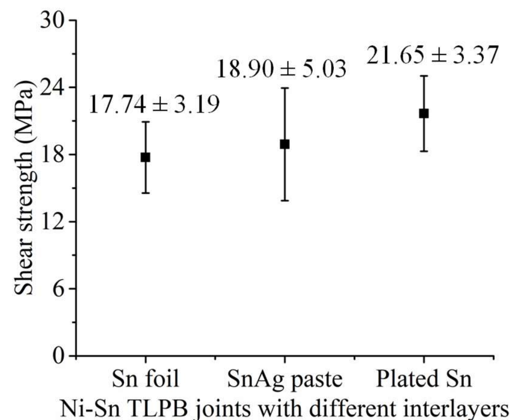

Fig. 5. Shear strength profiles of the Ni-Sn TLP bonded joints with different interlayers (Sn foil, $Sn_{96.5}Ag_{3.5}$ paste and electroplated Sn, bonded at 300 °C for 2 h).

Fig. 6 shows typical shear fractured surfaces of the Ni-Sn TLP bonded joints made using different interlayers after shear tests. Many voids can be found on the fracture surfaces of the joints made using Sn foil (Fig. 6(a)) and $Sn_{96.5}Ag_{3.5}$ paste (Fig. 6(b)), while fewer voids were found on the fracture morphology of the electroplated Ni-Sn TLP bonded joint (Fig. 6(c)). EDS

results proved that both remnant Sn and Ni_3Sn_4 IMCs were detected on the shear fractured surfaces of all joints. More remnant Sn was found on the fracture surface of the $Sn_{96.5}Ag_{3.5}$ paste joint, while there was hardly any remnant Sn on the fracture surface of the electroplated Sn joint. As a weak phase in the joint, the remnant Sn around the grain boundaries of Ni_3Sn_4 IMCs provides preferred sites for crack initiation and propagation, which led to the intergranular fracture of the joints during shear fracture tests. Intergranular fracture was found to be the dominant fracture mode for all the Ni-Sn TLP bonded joints made using different interlayers, while more transgranular fracture areas were observed on the fracture surface of the electroplated Ni-Sn TLP bonded joint. These phenomena reinforce the shear strength profiles of the joints shown in Fig. 5.

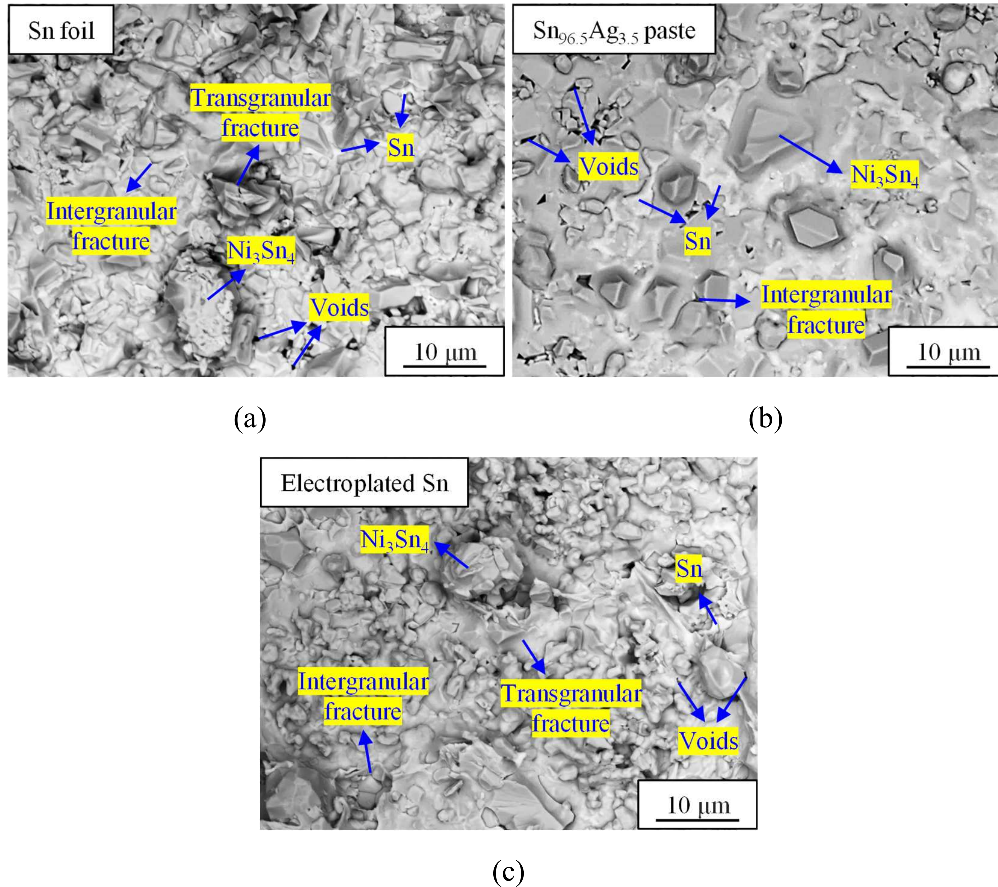

Fig. 6. Shear fractured surfaces of Ni-Sn TLP bonded joints made using different interlayers, (a) Sn foil, (b) $Sn_{96.5}Ag_{3.5}$ paste, and (c) electroplated Sn (bonded at 300 °C for 2 h).

3.2 The electroplated Ni-Sn TLP bonded joints with different bonding times

Fig. 7 shows combined band contrast and phase mappings of the cross-sectional microstructure of the electroplated Ni-Sn TLP bonding joints made with different bonding times. It can be observed that the area percentage of the Ni_3Sn_4 IMCs increased with increasing bonding time from 0.5 h to 5 h. Also, the average grain size of the formed Ni_3Sn_4 IMCs continuously increased with prolonged bonding times. Firstly, columnar-shaped Ni_3Sn_4 grains formed along the surface of the electroplated Ni towards the remnant Sn which was present as a single continuous layer around the centre of the joint after bonding for 0.5 h (Fig. 7(a)). Some grains grew faster than other grains in the joints, which might be due to their lower surface energy or

grain boundary energy [25-27]. Also, the newly formed fine Ni_3Sn_4 grains around the Ni/Ni_3Sn_4 interfaces are mainly along the grain boundaries of Ni_3Sn_4 IMCs because the grain boundary diffusion of Ni/Sn is much faster than the lattice diffusion [28]. It can be observed that there are some newly-formed fine Ni_3Sn_4 grains adjacent to the Ni/Ni_3Sn_4 interfaces in the joints bonded for 0.5 h and 1 h due to the faster diffusion of Sn compared to Ni [29], which confirms that the Ni/Ni_3Sn_4 interface was the preferential site for the nucleation of the newly formed Ni_3Sn_4 IMC grains during bonding. As the bonding time increased to 1 h, the Ni_3Sn_4 IMCs grew across the entire joint which resulted in the remnant Sn no longer being a continuous layer (Fig. 7(b)). Based on the studies of the growth mechanism of Ni_3Sn_4 IMCs reported by He et al. [30] and Tseng et al. [20], the grain boundary diffusion and grain growth (ripening) are the dominant growth mechanisms of the Ni_3Sn_4 IMCs in Ni-Sn joints. After the joint bonded for 2 h, only a small amount of remnant Sn was found around the grain boundaries of Ni_3Sn_4 IMCs (Fig. 7(c)). Accompanying the consumption of Sn, newly formed fine-grained Ni_3Sn_4 IMCs were observed around sites with remnant Sn until the Sn was fully consumed. The IPF(Y) mapping images indicate that the remnant Sn for each joint has a unified orientation in the Y direction that is close to its [001] direction. There is no preferred orientation of the Ni_3Sn_4 IMC grains formed in all joints. In addition, the KAM mappings of the joints show that the local average misorientations adjacent to the Sn/Ni_3Sn_4 interfaces were higher than in other areas. As the bonding time further increased to 5 h, the Sn was fully consumed and transformed to the Ni_3Sn_4 IMCs (Fig. 7(d)). Also, the joint area became more homogeneous.

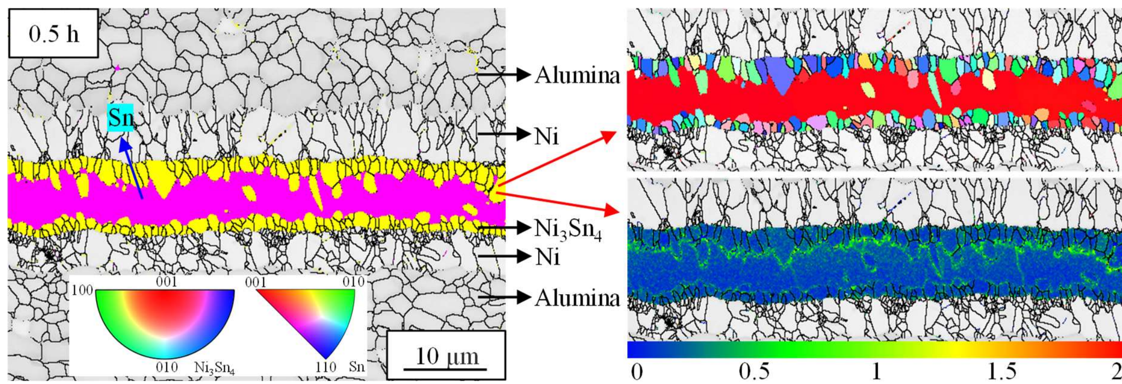

(a)

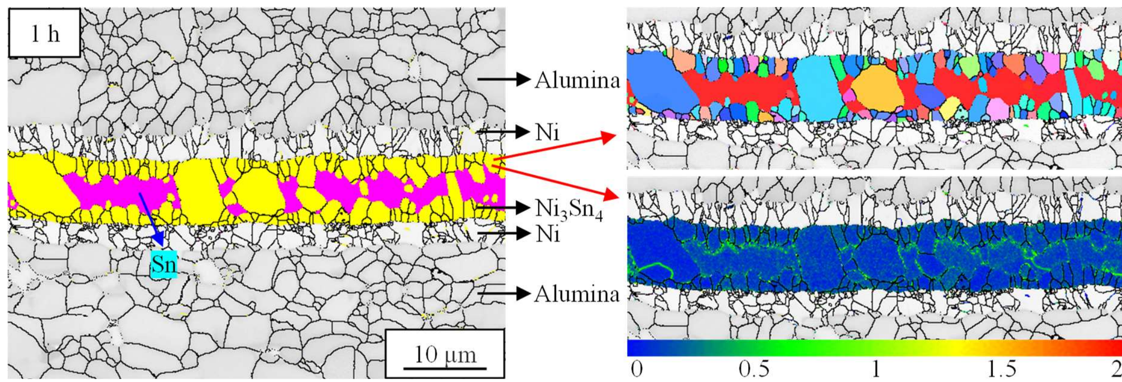

(b)

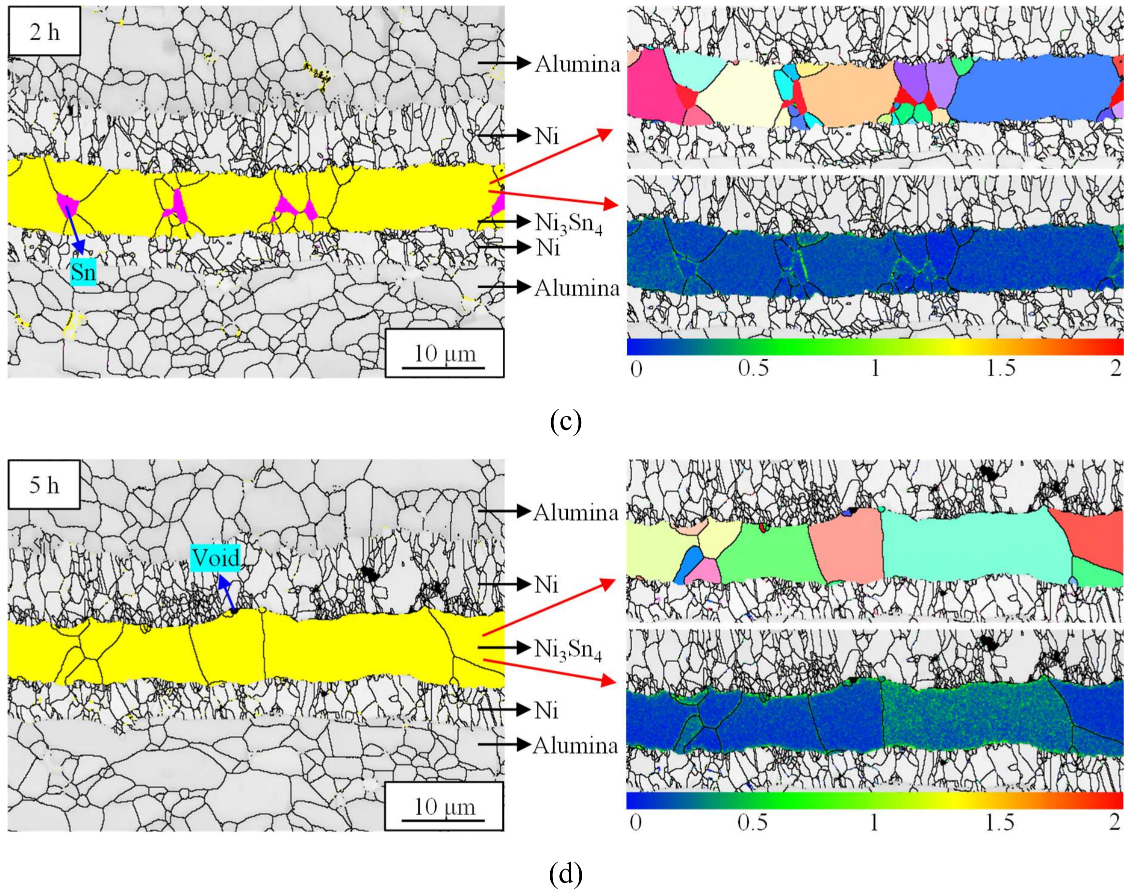

Fig. 7. Combined band contrast, phase, IPF(Y) and KAM mappings of the cross-sectional microstructure of electroplated Ni-Sn TLP bonded joints with different bonding times, (a) 0.5 h, (b) 1 h, (c) 2 h, and (d) 5 h (at 300 °C).

Fig. 8 shows that the average shear strength of the Ni-Sn TLP bonded joint continuously increased from 14.86 ± 3.68 MPa to 25.01 ± 5.96 MPa as the bonding time increased from 0.5 h to 5 h. The increment in the average shear strength with the bonding time from 0.5 h to 2 h was mainly attributed to the consumption of Sn with the prolonged bonding time. As the bonding time further increased to 5 h, the enhancement of the joint was mainly due to the remnant Sn being fully consumed, coalescence of the voids and the homogenization of the joint.

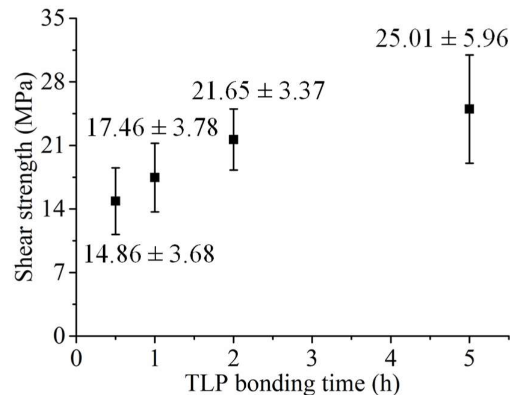

Fig. 8. Shear strength profiles of the electroplated Ni-Sn TLP bonding joints under different bonding times (at 300 °C).

Typical shear fractured surfaces of the electroplated Ni-Sn TLP bonded joints made with different bonding times are shown in Fig. 9. Large areas of remnant Sn with a few scattered Ni_3Sn_4 IMCs were revealed on the fracture surface of the Ni-Sn TLP bonded joint after bonding for 0.5 h. Sn failed through ductile fracture and a few voids were detected around the Ni_3Sn_4 IMCs (Fig. 9(a)). Alternately distributed Ni_3Sn_4 IMCs and remnant Sn were observed on the fracture surface of the joint bonded for 1 h. Failure of Ni_3Sn_4 IMCs was mainly through intergranular fracture (Fig. 9(b)). More voids were found on the fracture surfaces of the joints bonded for 1 h and 2 h due to the continuous volume shrinkage caused by phase transformation [31]. In addition, small areas of remnant Sn were detected on the fracture surface of the joint bonded for 2 h, which resulted in intergranular fracture (Fig. 9(c)). Besides, many transgranular fracture areas were revealed on the fracture surface as well. As the bonding time further increased to 5 h, the fracture surface was composed of fully formed Ni_3Sn_4 IMCs which failed mainly due to transgranular fracture (Fig. 9(d)). Also, fewer voids were found due to the coalescence and shrinking of voids [31].

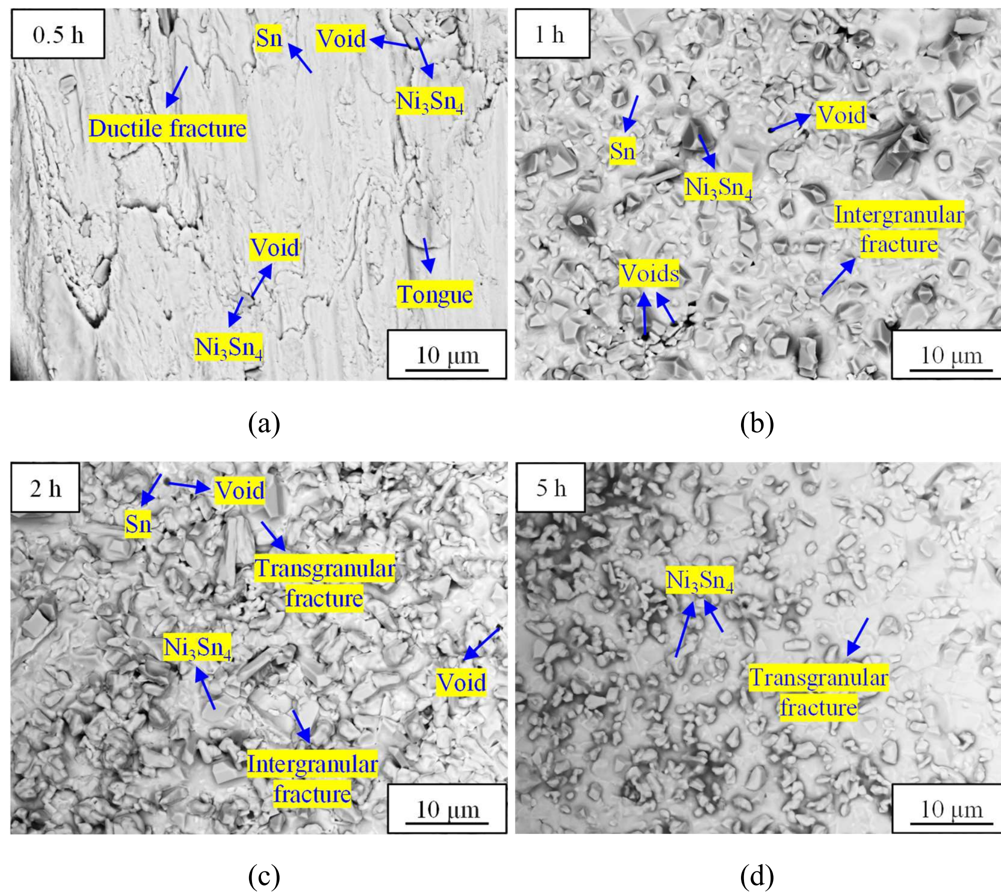

Fig. 9. Shear fracture surfaces of the electroplated Ni-Sn TLP bonded joints made with different bonding times, (a) 0.5 h, (b) 1 h, (c) 2 h, and (d) 5 h (at 300 °C).

3.3 The electroplated Ni-Sn TLP bonded joints with different aging times

Fig. 10 shows combined band contrast and phase mappings of the cross-sectional microstructure of the electroplated Ni-Sn TLP bonded joints subjected to different aging times. No Ni_3Sn_2 IMC was detected in the microstructure of the joint after aging for 4 h, while scattered Ni_3Sn_2 IMCs (green) were detected between the Ni and Ni_3Sn_4 after aging for 10 h

(due to the limitation of the resolution of EBSD scanning). A thin layer (the average thickness is around 0.64 μm) of nano-sized Ni_3Sn_2 IMCs was found on the joint after aging for 25 h. The average thickness of the Ni_3Sn_2 IMCs layer increased to 0.75 μm and 1.36 μm after aging for 50 h and 100 h, respectively. Also, the mean grain size of the Ni_3Sn_2 IMCs increased as aging time was prolonged from 10 h to 100 h. It can be observed in Fig. 10(d) and (e) that the Ni_3Sn_2 IMC grains around the Ni/Ni_3Sn_2 interface are finer than other regions, which indicates that the Ni/Ni_3Sn_2 interface was the preferential site for nucleation of the newly formed Ni_3Sn_2 IMC grains. This phenomenon was due to the faster diffusion of Sn as compared to Ni [28]. In addition, a thin wedge-shaped void was observed along the grain boundary of Ni_3Sn_4 IMCs after aging for 25 h (Fig. 10(c)). Larger voids were found along the grain boundaries of Ni_3Sn_4 IMCs as the aging time was prolonged to 50 h and 100 h. The formation and enlargement of these voids can be attributed to volume shrinkage caused by the phase transformation from Ni_3Sn_4 to Ni_3Sn_2. There was no preferred orientation of the newly formed Ni_3Sn_2 IMCs in the joint after long-term aging, as shown in the IPF(Y) mappings in Fig. 10(d) and (e). Furthermore, the KAM mappings in Fig. 10(d) and (e) indicate that the local average misorientation around the Ni/Ni_3Sn_2 interface is higher than that in the Ni_3Sn_2 IMCs region and the local average misorientation around the Ni_3Sn_2/Ni_3Sn_4 interface is higher than that in the Ni_3Sn_4 IMCs area. These indicate the potential lattice stress around the Ni/Ni_3Sn_2 interface is higher than that in the Ni_3Sn_2 IMCs region and the stress around the Ni_3Sn_2/Ni_3Sn_4 interface is higher than that in the Ni_3Sn_4 IMCs area [23, 24].

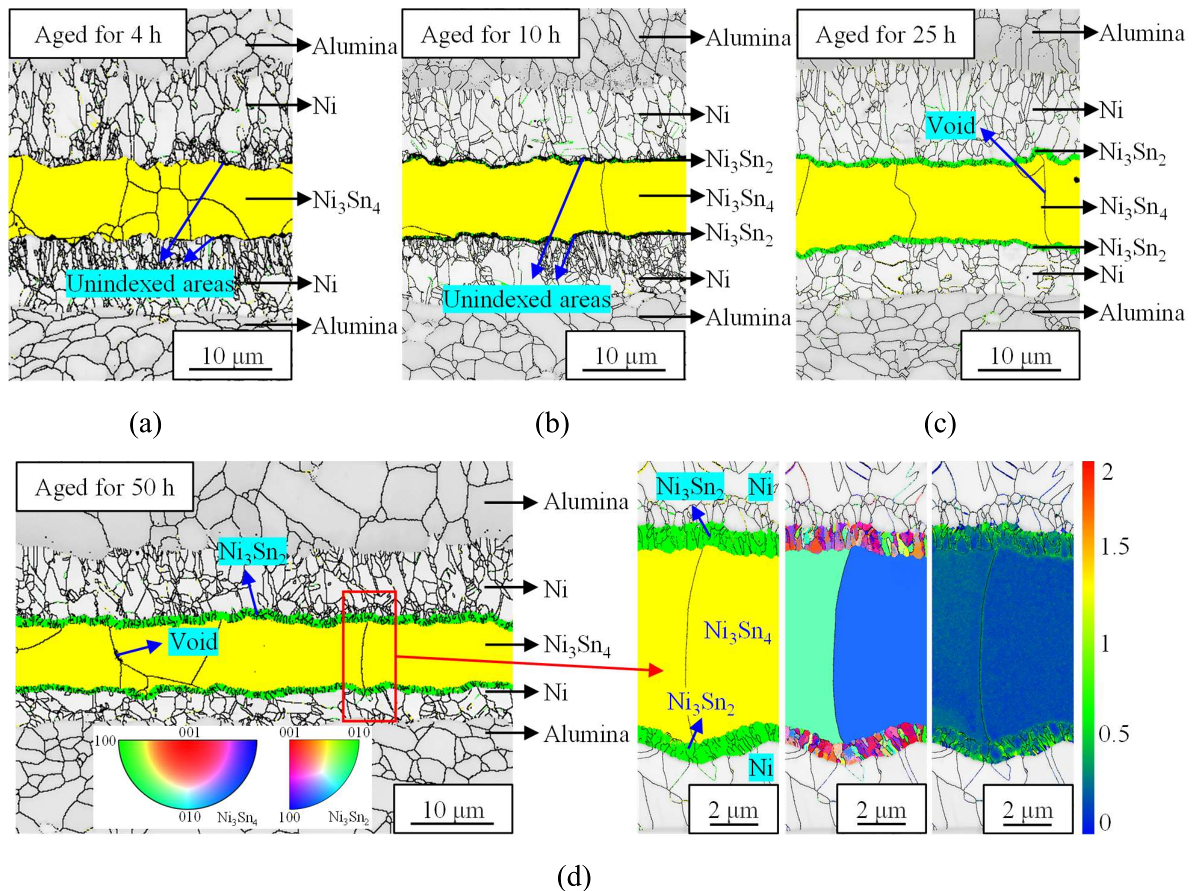

(d)

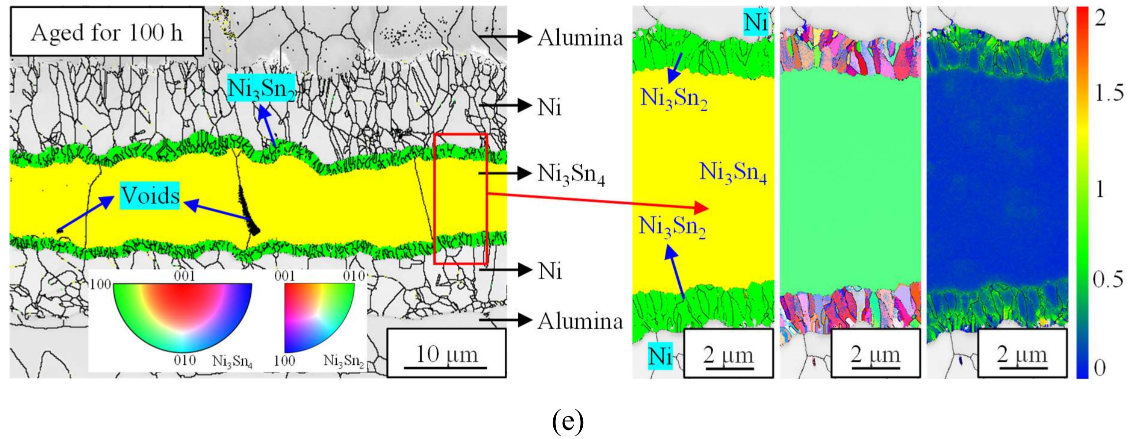

(e)

Fig. 10. Combined EBSD mappings of the cross-sectional microstructure of the electroplated Ni-Sn TLP bonded joints prepared with different aging times, (a) 4 h, (b) 10 h, (c) 25 h, (d) 50 h, and (e) 100 h (at 300 °C).

Fig. 11 shows the average shear strength profiles of the electroplated Ni-Sn TLP bonded joints after aging for 0 h (as-bonded), 4 h, 10 h, 25 h, 50 h and 100 h. The average shear strengths of the joints after aging for 0 h, 4 h, 10 h, 25 h, 50 h and 100 h are 17.46 ± 3.78 MPa, 22.82 ± 6.35 MPa, 20.51 ± 5.54 MPa, 17.96 ± 4.49 MPa, 16.94 ± 3.42 MPa and 15.22 ± 3.81 MPa, respectively. The increase in the average shear strength of the joints after aging for 4 h (compared to the as-bonded joint) was mainly due to the consumption of remnant Sn (refer to Fig. 7(b) and Fig. 10(a)), while the decrease in the strength of the joints after aging for 10 h might be attributed to the phase transformation from Ni_3Sn_4 to Ni_3Sn_2, which has resulted in the formation of voids. The further continuous decrease of the joints after aging for 25 h to 100 h was mainly attributed to the formation and enlargement of voids with the prolonged aging time.

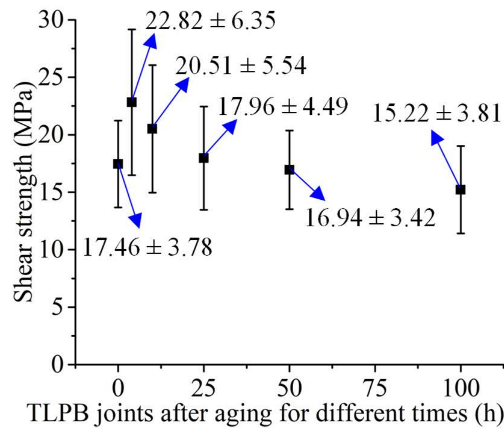

Fig. 11. Shear strength profiles of the electroplated Ni-Sn TLP bonded joints after aging for different times (at 300 ℃).

Fig. 12 shows the cross-sectional microstructure and fracture surfaces of the shear fractured electroplated Ni-Sn TLP bonded joints after different aging times. The cross-sectional microstructure in Fig. 12(a), (b), (c), (d) and (e) indicates that the aged joints fractured through both the Ni_3Sn_4 IMCs and the Ni_3Sn_2/Ni_3Sn_4 interface during shear tests. Take the joints aged for 50 h and 100 h for examples, the top-view fracture surfaces indicate that some regions of

the shear fractured surfaces are fully covered by the Ni_3Sn_4 IMCs (fractured through the Ni_3Sn_4 IMCs, Fig. 12(f) and (g)), while others contain large areas of Ni_3Sn_2 IMCs with Ni_3Sn_4 IMCs embedded in between (fractured through the Ni_3Sn_2/Ni_3Sn_4 interface, Fig. 12(h) and (i)). Voids were observed around the grain boundaries of Ni_3Sn_4 IMCs on the fractured Ni_3Sn_4 IMCs side of the joint after aging for 50 h (Fig. 12(f)) and the voids were enlarged as the aging time increased to 100 h (Fig. 12(g)). This is in accordance with the phase mappings shown in Fig. 10(d) and (e). In addition, nanovoids were found on the fracture surface of the Ni_3Sn_2/Ni_3Sn_4 interface of the joint aged for 50 h (Fig. 12(h)), and more nanovoids were observed on that of the joint aged for 100 h (Fig. 12(i)). The formation of nanovoids around the Ni_3Sn_2/Ni_3Sn_4 interface was due to the uneven interdiffusion of Ni/Sn during the phase transformation from Ni_3Sn_4 to Ni_3Sn_2 [32]. The fracture that propagated through the Ni_3Sn_4 IMCs was mainly due to the voids formed and enlarged around the grain boundaries of the Ni_3Sn_4 IMCs during the long-term aging process. While the fracture along the Ni_3Sn_2/Ni_3Sn_4 interface might partially be attributed to the relatively higher stress concentration around the Ni_3Sn_2/Ni_3Sn_4 interface induced by the phase transformation (Fig. 10(d) and (e)). To some extent, the elastic anisotropy mismatch between Ni_3Sn_4 and Ni_3Sn_2 IMCs might also contribute to the interfacial cracking during the shear tests [33]. Besides, the nanovoids formed around the Ni_3Sn_2/Ni_3Sn_4 interface might also have resulted in the degradation in the mechanical strength of the interface. Though higher residual stresses were found in the Ni_3Sn_2 IMCs regions than that in the Ni_3Sn_2/Ni_3Sn_4 interface (Fig. 10(d) and (e)), the isotropic nano-sized Ni_3Sn_2 IMCs exhibited higher mechanical strength than that of the Ni_3Sn_2/Ni_3Sn_4 interface. It was observed that intergranular fracture was the dominant fracture mode for the joints after aging for 50 h and 100 h. Fig. 12(j) and (k) show the corresponding EDS mappings of oxygen for the fractured Ni_3Sn_4 sides of the joints after aging for 50 h and 100 h (corresponding to Fig. 12(f) and (g)), respectively. It is shown that the concentration of oxygen (yellow) around the grain boundary area (brighter) was higher than that of the Ni_3Sn_4 IMCs region (darker) as the oxygen diffuses faster along the voids and grain boundaries than that across the IMCs [28]. Also, there was an increment in the average weight percentage of the oxygen of the fracture surface for the fractured Ni_3Sn_4 side when the aging time increased from 50 h (8.5 wt.%) to 100 h (11.9 wt.%), and the fracture surfaces revealed the Ni_3Sn_2/Ni_3Sn_4 interface presented much lower average weight percentages of oxygen in the joints after aging for 50 h (4.2 wt.%) and 100 h (4.6 wt.%). The continuous degradation in the average shear strength of the joints with the prolonged aging time was partially attributed to the increased oxidation in the joints as the brittle oxides are preferred sites for crack initiation and propagation [34].

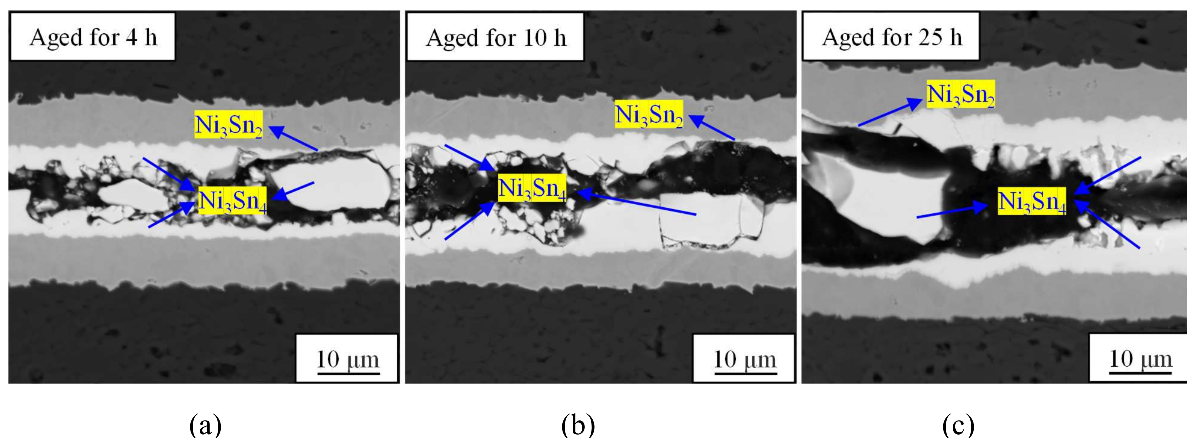

(a) (b) (c)

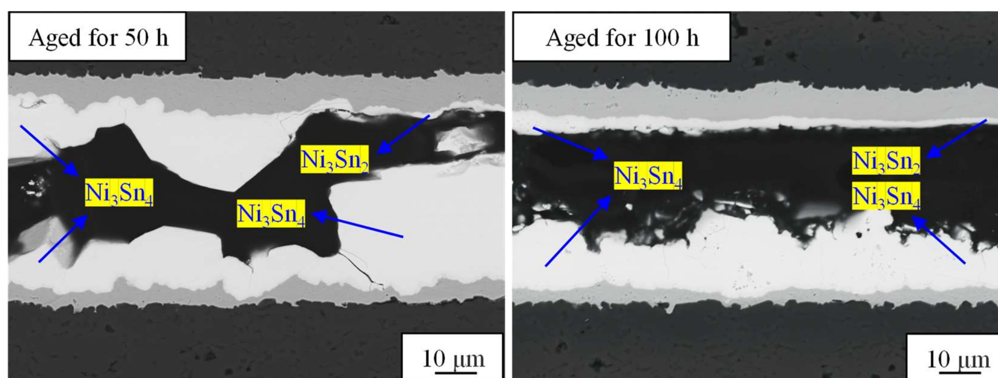

(d) (e)

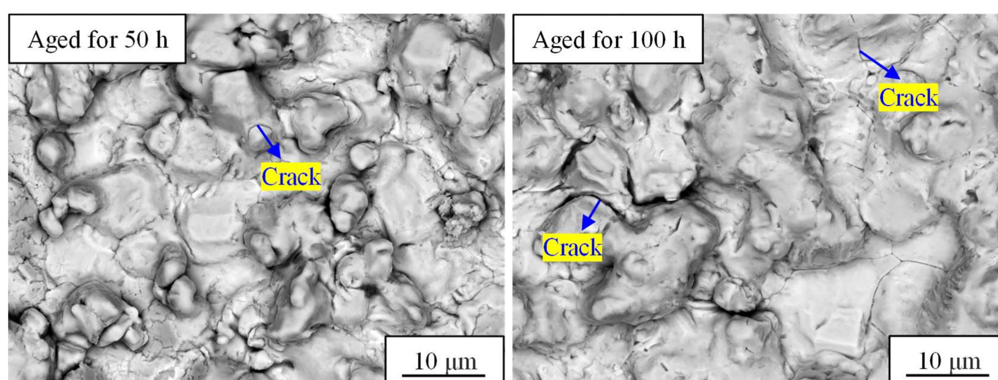

(f) (g)

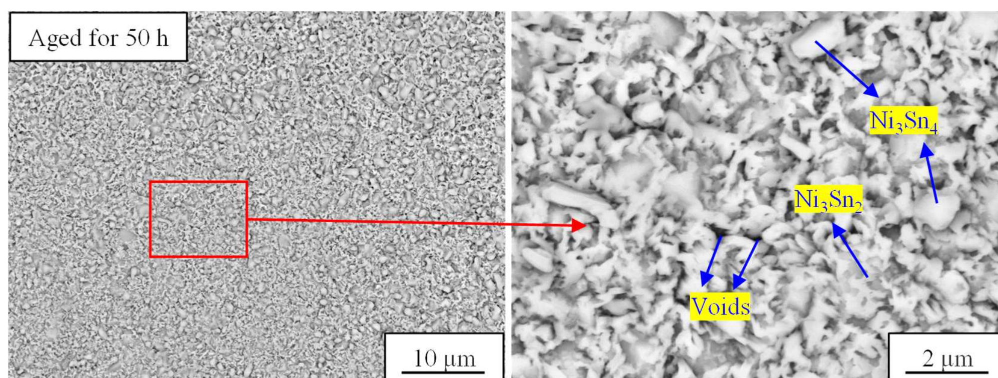

(h)

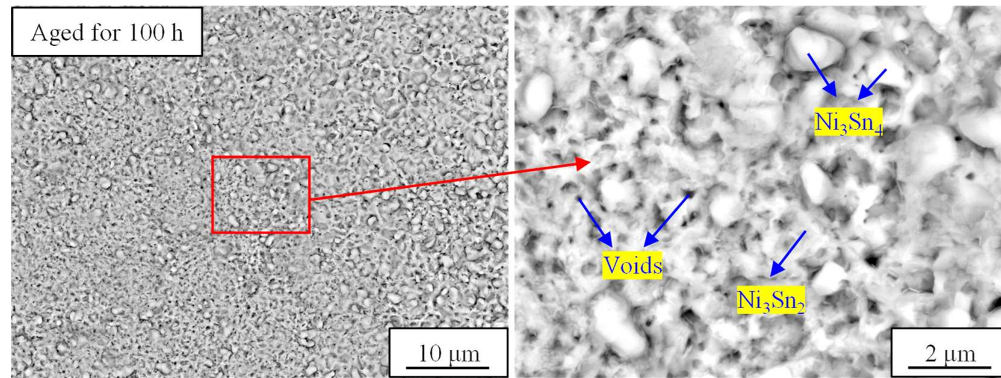

(i)

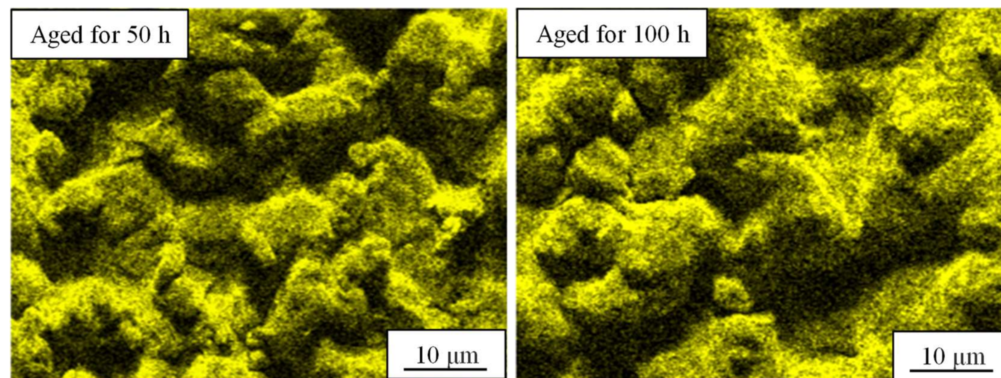

(j) (k)

Fig. 12. Cross-sectional microstructure of the shear fractured electroplated Ni-Sn TLP bonded joints after aging for (a) 4 h, (b) 10 h, (c) 25 h, (d) 50 h, and (e) 100 h (at 300 °C); shear fractured surfaces that fractured through Ni_3Sn_4 IMCs of the joints after aging for (f) 50 h, (g) 100 h, fractured through the Ni_3Sn_2/Ni_3Sn_4 interface after aging for (h) 50 h, (i) 100 h; and the corresponding EDS mappings of oxygen for the shear fractured surfaces that fractured through Ni_3Sn_4 IMCs of the joints after aging for (j) 50 h, and (k) 100 h (corresponding to Fig. 12(f) and (g), respectively).

4 Conclusions

Electroplated Ni-Sn TLP bonded joints were studied in this work for potential applications in high-temperature electronic packaging. A comparative study of Ni-Sn joints that used different types of interlayers was performed. In-depth analyses of the evolution of microstructure and mechanical properties in electroplated Ni-Sn TLP joints made with different bonding and aging times were also conducted. Several main conclusions can be made:

1) The average shear strength of Ni-Sn TLP bonded joints made using electroplated Sn as the interlayer was slightly higher than the ones made using Sn foil and $Sn_{96.5}Ag_{3.5}$ paste. This was due to there being more voids formed in the Sn foil joint. Also, it is challenging to control the amount of $Sn_{96.5}Ag_{3.5}$ paste applied for TLP bonding. Excess paste resulted in more remnant Sn in the joint after bonding, which deteriorated the shear strength of the joint.

2) The average shear strength of the electroplated Ni-Sn TLP bonded joints continuously increased as the bonding time increased from 0.5 h to 5 h, while it decreased as the aging time was prolonged from 4 h to 100 h. The increment in the strength as the bonding time increased was mainly due to the consumption of Sn and the homogenization of the joint. The continuous degradation in the strength of the joint as the aging time from 4 h to 100 h was attributed to the combined effects of void formation and enlargement, and the increased oxidation of the joints with prolonged aging time.
3) The Ni/Ni_3Sn_4 interface was the preferential site for the nucleation of the newly formed Ni_3Sn_4 IMC grains during bonding and the mean grain size of Ni_3Sn_4 continuously increased with the increasing bonding time. In addition, nano-sized Ni_3Sn_2 IMC grains were found in the electroplated Ni-Sn TLP bonded joint after aging for 10 h and were enlarged as the aging time further increased to 100 h. Furthermore, the Ni/Ni_3Sn_2 interface was the preferential site for the nucleation of newly formed Ni_3Sn_2 IMC grains in the joints during aging.
4) Intergranular fracture was the dominant fracture mode in the sheared electroplated Ni-Sn TLP bonded joints after high-temperature and long-term aging (at 300 ℃ for 50 h and 100 h). In addition, the shear fractures of the aged joints propagated through both the Ni_3Sn_4 IMCs and the Ni_3Sn_2/Ni_3Sn_4 IMCs interface.

Acknowledgements

The work was investigated with the support of Rolls-Royce@NTU Corporate Laboratory, Nanyang Technological University and the National Research Foundation (NRF). We would also like to acknowledge the Facility for Analysis, Characterisation, Testing and Simulation (FACTS), Nanyang Technological University, Singapore, for use of their facilities. In addition, the help from Dr Li Wei at MAE, NTU for preparing EBSD samples is also acknowledged.

Data availability statement

The data that support the findings of this study are available from the authors upon reasonable request.

References

[1] A. Sharif, C.L. Gan, Z. Chen, Transient liquid phase Ag-based solder technology for high-temperature packaging applications, Journal of Alloys and Compounds, 587 (2014) 365-368.

[2] J.R. Holaday, C.A. Handwerker, Transient Liquid Phase Bonding, in: K.S. Siow (Ed.) Die-Attach Materials for High Temperature Applications in Microelectronics Packaging: Materials, Processes, Equipment, and Reliability, Springer International Publishing, Cham, 2019, pp. 197-249.

[3] L. Zhang, Z. Liu, Inhibition of intermetallic compounds growth at Sn-58Bi/Cu interface bearing CuZnAl memory particles (2-6 μm), Journal of Materials Science: Materials in Electronics, 31 (2020) 2466-2480.

[4] L. Sun, L. Zhang, C. Wei, M. Chen, Y. Zhang, Transient liquid phase bonding (TLPB) of Cu to Cu using Sn interconnect solder reinforced by submicron Al particles, Journal of Materials Processing Technology, 307 (2022) 117686.

[5] L. Sun, M. Chen, L. Zhang, Microstructure evolution and grain orientation of IMC in Cu-Sn TLP bonding solder joints, Journal of Alloys and Compounds, 786 (2019) 677-687.

[6] X. Hu, H. Xu, W. Chen, X. Jiang, Effects of ultrasonic treatment on mechanical properties and microstructure evolution of the Cu/SAC305 solder joints, Journal of Manufacturing Processes, 64 (2021) 648-654.

[7] X. Peng, Y. Wang, Z. Ye, J. Huang, J. Yang, S. Chen, X. Zhao, Microstructural evolution and performance of high-tin-content $Cu_{40}Sn_{60}$ (wt.%) core/shell powder TLPS bonding joints, Journal of Manufacturing Processes, 75 (2022) 853-862.

[8] N.S. Nobeen, G. Yan, C.L. Gan, Z. Chen, Ag-Sn Transient Liquid Phase Bonding for High Temperature Electronic Packaging: Effect of Ag Content, IEEE Transactions on Components, Packaging and Manufacturing Technology, 10 (2020) 1604-1610.

[9] H. Shao, A. Wu, Y. Bao, Y. Zhao, G. Zou, Microstructure characterization and mechanical behavior for Ag_3Sn joint produced by foil-based TLP bonding in air atmosphere, Materials Science and Engineering: A, 680 (2017) 221-231.

[10] S.W. Yoon, M.D. Glover, K. Shiozaki, Nickel-tin transient liquid phase bonding toward high-temperature operational power electronics in electrified vehicles, IEEE Transactions on Power Electronics, 28 (2012) 2448-2456.

[11] K.D. Min, C.J. Lee, B.U. Hwang, J.H. Kim, J.H. Jang, S.B. Jung, Hybrid transient liquid phase sintering bonding of Sn-3.0Ag-0.5Cu solder with added Cu and Ni for CuNi bonding, Applied Surface Science, 551 (2021) 149396.

[12] H. Dong, Z. Li, X. Song, H. Zhao, H. Tian, J. Liu, J. Yan, Grain morphology evolution and mechanical strength change of intermetallic joints formed in Ni/Sn/Cu system with variety of transient liquid phase soldering temperatures, Materials Science and Engineering: A, 705 (2017) 360-365.

[13] D. Jung, A. Sharma, M. Mayer, J. Jung, A review on recent advances in transient liquid phase (TLP) bonding for thermoelectric power module, Reviews on advanced materials science, 53 (2018) 147-160.

[14] H. Zhao, J. Liu, Z. Li, X. Song, Y. Zhao, H. Niu, H. Tian, H. Dong, J. Feng, A comparative study on the microstructure and mechanical properties of Cu_6Sn_5 and Cu_3Sn joints formed by TLP soldering with/without the assistance of ultrasonic waves, Metallurgical and Materials Transactions A, 49 (2018) 2739-2749.

[15] H. Shao, A. Wu, Y. Bao, Y. Zhao, L. Liu, G. Zou, Rapid Ag/Sn/Ag transient liquid phase bonding for high-temperature power devices packaging by the assistance of ultrasound, Ultrasonics Sonochemistry, 37 (2017) 561-570.

[16] Z. Li, H. Dong, X. Song, H. Zhao, J. Feng, J. Liu, H. Tian, S. Wang, Rapid formation of Ni_3Sn_4 joints for die attachment of SiC-based high temperature power devices using ultrasound-induced transient liquid phase bonding process, Ultrasonics Sonochemistry, 36 (2017) 420-426.

[17] J. Shen, Y.C. Chan, S. Liu, Growth mechanism of Ni_3Sn_4 in a Sn/Ni liquid/solid interfacial reaction, Acta Materialia, 57 (2009) 5196-5206.

[18] S.E. Jeong, S.B. Jung, J.W. Yoon, High-temperature stability of Ni-Sn intermetallic joints for power device packaging, Journal of Alloys and Compounds, 890 (2022) 161778.

[19] K. Chu, C. Lee, S.H. Park, Y. Sohn, Effects of Ag addition and Ag_3Sn formation on the mechanical reliability of Ni/Sn solder joints, Microelectronics Reliability, 75 (2017) 53-58.

[20] Y.C. Tseng, H. Lee, S.C. Tsai, Y.W. Yen, C.M. Chen, Suppression effect of Ni grain size on the Ni_3Sn_4 growth at the Sn/Ni interface, Materials Characterization, 128 (2017) 232-237.

[21] H. Chuang, J. Yu, M. Kuo, H. Tong, C. Kao, Elimination of voids in reactions between Ni and Sn: a novel effect of silver, Scripta Materialia, 66 (2012) 171-174.

[22] A. Lis, C. Kenel, C. Leinenbach, Characteristics of reactive Ni_3Sn_4 formation and growth in Ni-Sn interlayer systems, Metallurgical and Materials Transactions A, 47 (2016) 2596-2608.

[23] L. Jiang, X. Ye, C. Cui, H. Huang, B. Leng, Z. Li, X. Zhou, Intermediate temperature embrittlement of one new Ni-26W-6Cr based superalloy for molten salt reactors, Materials Science and Engineering: A, 668 (2016) 137-145.

[24] G. Yan, B. Nagarajan, A. Bhowmik, S.C. Tan, R. Xu, M.J. Tan, Induction transient liquid phase bonding of Inconel 718 with the nickel-based sintered brazing preform, Applied Surface Science, 473 (2019) 1024-1037.

[25] Y. Zheng, Y. Cheng, R. Huang, R. Qi, F. Rao, K. Ding, W. Yin, S. Song, W. Liu, Z. Song, Surface energy driven cubic-to-hexagonal grain growth of $Ge_2Sb_2Te_5$ thin film, Scientific reports, 7 (2017) 1-8.

[26] X. Zhong, D.J. Rowenhorst, H. Beladi, G.S. Rohrer, The five-parameter grain boundary curvature distribution in an austenitic and ferritic steel, Acta Materialia, 123 (2017) 136-145.

[27] H. Salama, J. Kundin, O. Shchyglo, V. Mohles, K. Marquardt, I. Steinbach, Role of inclination dependence of grain boundary energy on the microstructure evolution during grain growth, Acta Materialia, 188 (2020) 641-651.

[28] P. Van Uffelen, M. Suzuki, 3.19 - Oxide Fuel Performance Modeling and Simulations, in: R.J.M. Konings (Ed.) Comprehensive Nuclear Materials, Elsevier, Oxford, 2012, pp. 535-577.

[29] Y. Yang, J. Balaraju, Y. Huang, Y.Y. Tay, Y. Shen, Z. Tsakadze, Z. Chen, Interface Reaction Between Electroless Ni-Sn-P Metallization and Lead-Free Sn-3.5Ag Solder with Suppressed Ni_3P Formation, Journal of electronic materials, 43 (2014) 4103-4110.

[30] M. He, Z. Chen, G. Qi, Solid state interfacial reaction of Sn-37Pb and Sn-3.5Ag solders with Ni-P under bump metallization, Acta Materialia, 52 (2004) 2047-2056.

[31] H.L. Feng, J.H. Huang, J. Yang, S.K. Zhou, R. Zhang, Y. Wang, S. H. Chen, Investigation of microstructural evolution and electrical properties for Ni-Sn transient liquid-phase sintering bonding, Electronic Materials Letters, 13 (2017) 489-496.

[32] B. Horváth, B. Illés, T. Shinohara, Growth of intermetallics between Sn/Ni/Cu, Sn/Ag/Cu and Sn/Cu layered structures, Thin solid films, 556 (2014) 345-353.

[33] K.B. Broberg, 4 - Elastostatic Cracks, in: K.B. Broberg (Ed.) Cracks and Fracture, Academic Press, San Diego, 1999, pp. 99-246.

[34] C.L. Chuang, M.F. Shu, Y.H. Tseng, The Effect of Nickel Oxidation Formed in the Interface of ENEPIG Structure for Flip Chip Technology, in: International Symposium on Microelectronics, International Microelectronics Assembly and Packaging Society, 2018, pp. 000146-000152.